Korean Journal of Chemical Engineering (2024) 41:2449–2458
https://doi.org/10.1007/s11814-024-00161-x

ORIGINAL ARTICLE

Comparison and Analysis of Mixing Efficiency in Various Micromixer Designs

Seo yeon Oh[1] · Chang-Soo Lee[1]

Received: 22 January 2024 / Revised: 18 March 2024 / Accepted: 20 March 2024 / Published online: 26 March 2024

Abstract
In this paper, we evaluate the influence of various micromixer designs on the mixing efficiency of passive micromixers. We analyze the designs of various passive micromixers to identify the most efficient micromixer. Among them, the toroidal micromixer and 3D zig-zag micromixer demonstrated the highest mixing efficiency. We investigated the key factors influencing mixing in the toroidal and 3D zig-zag micromixer, identifying and confirming optimal designs. Ultimately, when comparing the mixing efficiency of the two micromixers, the 3D zig-zag micromixer achieved full mixing in a very short time of 0.8 ms. Through this research, it is anticipated that a benchmark will be provided for micromixer design in microfluidic devices when manufacturing micromixers of various forms.

Keywords Microfluidic system · Passive micromixer · Laminar flow · Enhancing mixing efficiency · Microchannel design

Introduction

Microfluidic systems play an important role in various application fields. In impacted on industries, such as environmental science, drug delivery, and biochemistry [1–8]. Recently, with the global pandemic of COVID-19, there has been active development of mRNA vaccines. Notably, the utilization of lipid nanoparticles (LNPs) in RNA delivery technology has a crucial role in the application of mRNA vaccines [9–11]. Macroscale LNP formation technologies are commonly used for convenience. However, achieving precise control over the size and polydispersity of liposomes poses inherent challenges for these techniques [12]. On the other hand, within microfluidic devices, the formation of LNPs using micromixers efficiently utilizes the surface and structure of microchannels for effective mixing, resulting in LNPs with an exceptional particle-size distribution. This methodology has attracted considerable attention from the biomedical industry and the fundamental biology and chemistry research area fields [13, 14].

In microfluidic systems, the microchannels exhibit a high surface area-to-volume ratio, leading to enhanced mass density and heat transfer and faster reaction rates. Furthermore, the handling of small fluid volumes provides the advantage of reduced reagents and energy consumption [15, 16]. The rapid and uniform mixing of two or more samples within these microchannels is crucially utilized in various applications, including biomedical analysis and synthesis [17].

To investigate the transient events occurring during chemical/biological processes on a microscale or to achieve optimal synthesizing results, rapid mixing within milliseconds before the reaction proceeds is essential [18]. However, the fluid flow in microchannels typically cannot generate turbulent flow and exhibits a laminar flow, resulting in a low Reynolds number (Re) [19]. Re is defined as

$$Re = \frac{\rho V D}{\mu},$$

where ρ is the density of the fluid, V is the velocity of the fluid, D is the characteristic length, and μ is the fluid dynamic viscosity.

In microfluidic device, the characteristic length (D) and the fluid velocity (V) are relatively small. Consequently, mixing in microfluidic devices occurs through molecular diffusion based on concentration gradients. This leads to an increased mixing

✉ Chang-Soo Lee
rhadum@cnu.ac.kr

Seo yeon Oh
dhtjdus98@naver.com

1 Department of Chemical Engineering and Applied Chemistry, Chungnam National University, 99, Daehak-Ro, Yuseong-Gu, Daejeon 34134, Korea

time and increases the microchannels length [20]. Therefore, in numerous studies, various designs of micromixers have been developed to enhance the mixing efficiency in a short mixing channel [21]. In general, micromixers can be classified into active and passive, depending on the application of external forces. Active micromixers utilize external energy sources, such as electric force, magnetic force, and acoustic waves, to enhance mixing efficiency [22–26]. In microfluidic system, external energy sources are employed to control fluid flow and facilitate mixing, achieving faster mixing rates and increased efficiency. However, active micromixers, requiring connection to an external energy source, exhibit a relatively intricate structure. The device fabrication process is complex and involves high costs [27]. In contrast, passive micromixers utilize the inherent properties of fluid flow at the microscale for mixing without the need for external energy inputs. This is achieved by extending fluid interfaces with low-pressure drops and short mixing lengths or inducing chaotic flow, attracting significant interest [28–32]. Passive micromixers offer the advantages of simplicity in structure, ease of device fabrication, and independence from external energy sources. These mixers are typically designed in both 2-dimensional (2D) and 3-dimensional (3D) structures.

However, previous studies on passive micromixers focused on the improving mixing efficiency through unique geometric configurations, surface treatment, or the integration of obstacles within the fluidic pathways [33–37]. Thus, a notable gap persists in previous studies, and it is difficult to find a comprehensive comparison of these various designs under standardized conditions to determine the most effective approach for passive mixing in microfluidic devices. This lack of comparative analysis makes it difficult for researchers to select the optimal design for their specific applications, thereby impeding progress in the development and application of microfluidic technologies.

In this paper, we perform a systematic investigation into the mixing efficiency of various micromixers. By employing a consistent set of experimental conditions across all designs tested, this study is to provide a clear and objective comparison of their performance, thereby offering valuable into the most effective design principles for passive mixing in microfluidic device. This study not only contributes to the advancement of microfluidic technology but also aids in the optimization of its applications.

Materials and Methods

Device Fabrication

In this experiment, various micromixers were designed using AutoCAD (Autodesk). Subsequently, the designs were fabricated through photolithography and soft lithography techniques. Through photolithography, we create a master mold with a design pattern on a silicon wafer, allowing for continuous and repeated use in subsequent experiments. To obtain a microfluidic device from master molds, soft lithography technology is applied using polydimethylsiloxane (PDMS). An elastomer (Sylgard 184, Dow Corning) and curing agent were mixed at a ratio of 10:1 (w/w) to make PDMS. After pouring PDMS onto the fabricated master mold, a thermal curing process was conducted on a hot plate at 65 °C for over 4 h. To fabricate the 2-dimensional microfluidic device, the cured PDMS was then separated from the master mold and bonded to a bare PDMS substrate through oxygen plasma treatment. We construct all four sides of the channel using PDMS, so we utilized PDMS to form the bottom part of the microchannel. The PDMS substrate was formed by curing PDMS in a petri dish, and it was subsequently peeled off for use. In contrast, the 3-dimensional microfluidic device is configured by stacking 2D structures to create layers. During the photolithography process, two separate 2D structures are produced. Subsequently, for the fabrication of the 3-dimensional device, PDMS is demolded from each silicon wafer, and after oxygen plasma treatment, the PDMS structures are aligned and bonded at the junctions.

Experiment in Mixing

To conduct comparative experiments, we utilized Alexa Flour 568 and Deionized water. Alexa flour 568 was dissolved in deionized water to create a 1 μM solution. For injecting solutions into the microfluidic device, we used a syringe pump (Harvard Apparatus PHD-2000 Advance Syringe pump) to inject fluid at a rate of 1 mL/min into each inlet. Fluorescence images for mixing efficiency analysis were captured using an optical microscope (Nikon ECLIPSE TE200-U) and a CCD camera (CoolSNAP™ cf Monochrome). We obtained fluorescent images of each microchannel. Furthermore, cross-sectional mixing images were acquired using a confocal microscope (Nikon A1 confocal, Japan) to observe fluid mixing patterns within the microchannels when interacting solutions into the 3D zigzag micromixer.

Analysis of Mixing Efficiency

The analysis of mixing efficiency aimed to utilize the average fluorescence intensity and standard deviation obtained from analyzing the region of interest (ROI) in each micromixer. To quantitatively assess the mixing efficiency within our passive micromixer designs, we employed a fluorescence-based the equation [38]

$$M = \left(1 - \frac{\sigma}{\bar{I}}\right) \times 100\%;$$

$\bar{\boldsymbol{I}}$ represents the average fluorescence intensity measured in the region of interest (ROI), and $\boldsymbol{\sigma}$ is the standard deviation value of fluorescence intensity measured in the ROI.

Furthermore, to provide a more accurate representation of mixing performance, we normalize the mixing efficiency using the equation [39]

$$M_n = \frac{M_k - M_{min}}{M_{max} - M_{min}}.$$

In this formula, M_n represents the normalized mixing efficiency, M_k is the calculated mixing efficiency, M_{max} is the maximum observed mixing efficiencies, and M_{min} is the minimum observed mixing efficiencies, respectively. By normalizing the mixing efficiency, we effectively scale the values, such that 0 indicates no mixing, and 1 indicates complete mixing, facilitating a clearer comparison between different micromixer designs.

Results and Discussion

Design of Passive Micromixers

In previous studies, various passive micromixers have been proposed. In this study, to determine which design among passive micromixers achieves the most efficient mixing, we designed a total of 5 passive micromixers with different channel geometries (Table 1).

Table 1 Types of micromixer designs

Micromixer design	Scheme of micromixer
Straight	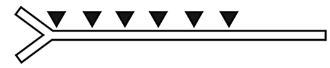
Serpentine**	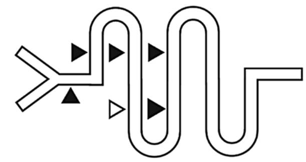
Herringbone	
3D zig-zag	
Toroidal	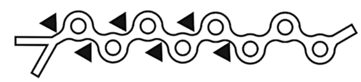

*The measurement points marked by closed triangles

**The open triangle represents the msec missing point in the serpentine micromixer

For passive micromixers with a 2D structure, we developed designs for straight, serpentine, herringbone [40], and toroidal [41] micromixers. For the 3D structure, we designed a 3D zig-zag micromixer [42, 43]. Additionally, we compared the M_n values for each micromixer design. The inlet and outlet of each micromixer were designed to be identical. To compare the M_n based on the structure of the micromixer, we designed them with variations only in the mixing region. Figure 1 shows the detailed structure of the designed micromixers. After designing each micromixer, we injected fluid with the same Reynolds number into each micromixer and compared the M_n at the same time.

Comparison and Analysis of Mixing Efficiency in Various Micromixers

In this study, we aimed to identify the most efficient design among micromixers with different designs. Figure 2 illustrates the M_n results of the five micromixers. To assess the M_n value in each micromixer, we measured the distance from the point where the two fluids meet to the ROI within the micromixer. This distance was then converted into time units for comparative analysis. In Fig. 2, the 3D zig-zag micromixer reached an M_n value of 1.0 at around 1.3 ms mixing time. In contrast, other micromixer designs did not reach within the same time. Even upon reaching the endpoint at 1.6 ms, the M_n did not attain a high value. This demonstrates that the M_n value is influenced by the microchannel design of each micromixer.

The straight micromixer relies on molecular diffusion at the fluid interface due to the absence of structural elements. However, this process is generally slow; the M_n value is observed to be low, around 0.01 [44]. The herringbone micromixer differs from the straight micromixer in that it features an asymmetric herringbone structure repeated on the bottom surface of the microchannel.

The herringbone structure consists of two connected channels of different lengths, one relatively long and the other short, designed asymmetrically. This herringbone structure indicates a helical flow pattern of the fluid within the microchannel, facilitating effective mixing [45, 46]. As a result, the M_n at the endpoint increased to around 0.54, indicating improved mixing performance compared to a straight micromixer. However, the M_n value did not reach or come close, even at the endpoint.

In the serpentine micromixer, as the two injected fluids traverse through a curved channel, secondary flow driven by centrifugal forces induces a dean flow pattern, causing the fluid to move from the inner side of the channel

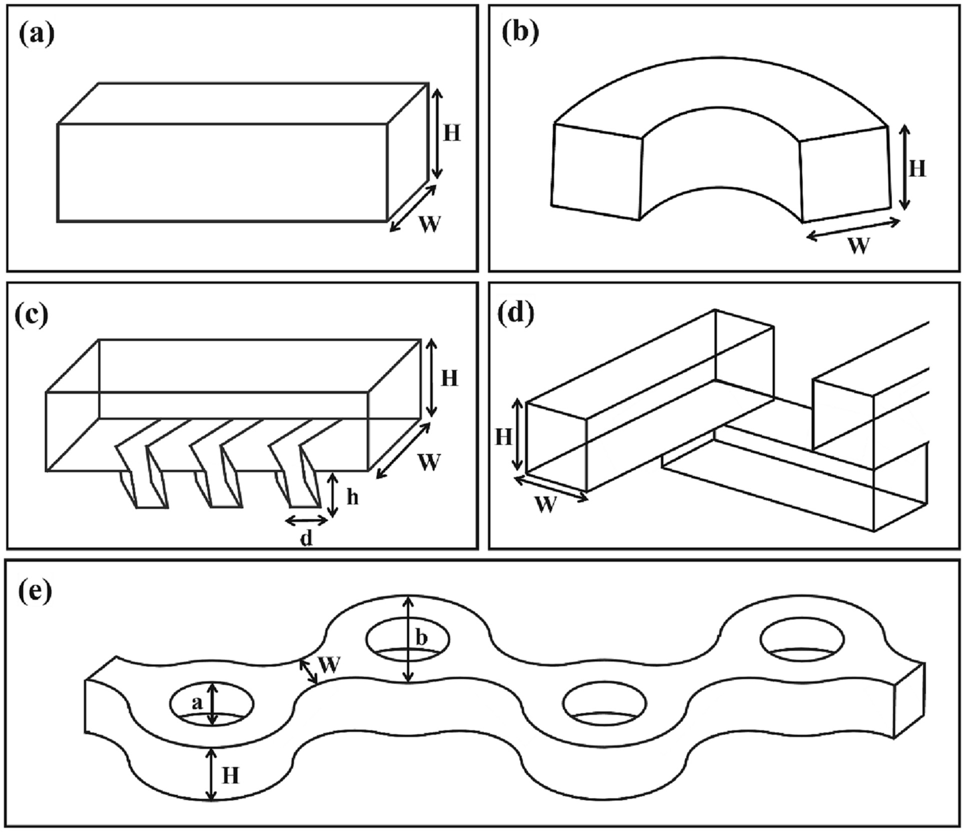

Fig. 1 The schematic drawing of each micromixer. **a** Straight micromixer. The channel height (H) and width (W) are 100 µm. The total length of the channel is 28 mm. **b** Serpentine micromixer. Both the height and width are 100 µm. The total length of the channel is 22 mm, and the number of repeat units is 4. **c** Herringbone micromixer. The channel has a height of 77 µm and a width of 100 µm. In the herringbone structure, height (h) is 23 µm, and the width **d** is 50 µm. The total length of the channel is 28 mm, and the number of repeat units is 8. **d** 3D zig-zag micromixer. Both the height and width are 100 µm. The total length of the channel is 23 mm, and the number of repeat units is 7. **e** Toroidal micromixer. Height (H) is 90 µm and width (W) is 110 µm. The inner circle of the toroidal micromixer (**a**) has a 330 µm, while the outer circle (**b**) has a 550 µm. The total length of the channel is 25 mm, and the number of repeat units is 8

toward the outer wall [47]. During this process, the fluids experience an increased interfacial area due to the curved geometry, leading to enhanced mixing efficiency. This results in more efficient mixing compared to the previous micromixer, with a confirmed M_n value of approximately 0.81 at the termination point. However, the M_n value exhibits a monotonic increase toward the later part of the microchannel due to the absence of obstacle within the microchannel, evenly saturating.

In the toroidal micromixer, fluid undergoes splitting induced by the toroidal shape, followed by recombination at the neck, resulting in asymmetric collisions that promote effective mixing [48]. Additionally, the toroidal micromixer, characterized by its repetitive pattern of spit and recombining, exhibits a substantial increase in the interfacial area where the fluids come into contact. This unique structure contributes to more effective mixing, resulting in an efficiency of approximately 0.88 at the outlet. Based on these results, the toroidal micromixer has

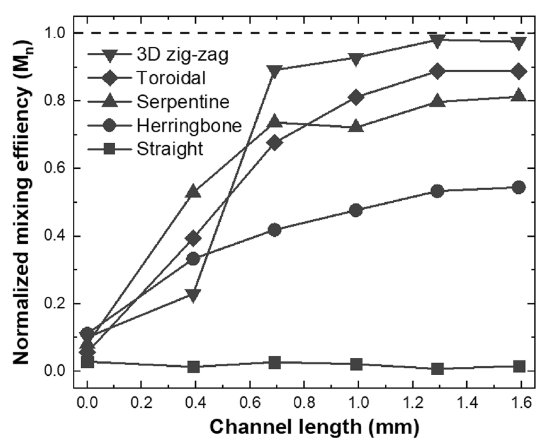

Fig. 2 Comparison of normalized mixing efficiency in various micromixer designs. The dashed line at the point where the normalized mixing efficiency value is 1.0 represents the criteria for the perfect mixing. The flow rates are fixed for all experiments with Re = 332

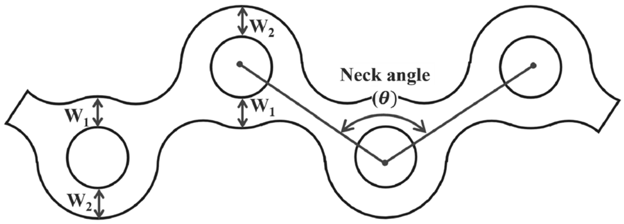

Fig. 3 Design of toroidal micromixer

Table 2 The design parameters of toroidal micromixer

Neck angle (θ)	90°	120°	140°	160°	180°
Width ratio (W1/W2)	1.0	2.0		3.0	4.0

been confirmed to exhibit the most efficient mixing among the micromixers with a two-dimensional structure.

Finally, the 3D zig-zag micromixer features a three-dimensional structure in contrast to the previous micromixers. The 3D structure induces also primary flow in the *x*–*y* plane and secondary flow in the vertical *z*-axis. This secondary flow enhances mixing by increasing the contact surface of the fluids. With this improved mixing, the 3D zig-zag micromixer achieves a M_n of approximately 0.98 at 1.3 ms, earlier than the endpoint at 1.6 ms.

Therefore, this paper, we aimed to modify the design parameters affecting M_n in the toroidal and 3D zig-zag micromixers. We optimized the design of toroidal and 3D zig-zag micromixer designs to confirm the most efficient one.

Experimental Assessment of Mixing in the Toroidal Micromixer with Various Designs

We anticipated that the neck angle (θ) and width ratio (W_1/W_2) in the toroidal micromixer would influence M_n, as illustrated in Fig. 3. Consequently, we modified each parameter to investigate the correlation with the parameters and M_n. Ultimately, we aimed to design the most efficient micromixer within the toroidal micromixer. As shown in Table 2, to investigate the influence of neck angle on M_n, we designed different neck angles (90°–180°), and we fixed the width ratio at 1.0. In designs with various width ratios, we fixed the neck angle at 120° and adjusted the width ratio (1.0–4.0).

To analyze M_n, we defined each section of the neck in the toroidal micromixer as a Region of Interest (ROI) and captured fluorescent images. The M_n was calculated using the average fluorescence intensity and standard deviation within the designated ROI.

First, the M_n of each micromixer with different neck angle was compared. Comparing the M_n values when the mixing time reached 1.4 ms, we observed respective values of 0.89, 0.78, 0.65, 0.5, and 0.25, respectively. At the endpoint (2.6 ms), the M_n values were calculated as 0.95, 0.95, 0.91, 0.83, and 0.5 for each design, respectively. Through these results, it was observed that as the neck angle approached 90°, the graph of M_n exhibited a rapid increase in values within a short time, saturating quickly (Fig. 4a). At the endpoint, a comparison of M_n at the smallest neck angle of 90° and the largest angle of 180° revealed that the M_n at a neck angle of 90° was approximately 90% higher than at 180°. In addition, as shown in Fig. 4b, an increase in the neck angle leads to a more distinct boundary between the two fluids. When fluid is injected into the toroidal micromixer, it undergoes split and recombination due to the structure of the microchannel. This process results in imbalanced collision and mixing. This is attributed to the fluid recombining at the neck section and causing collisions, which become more imbalanced when the neck angle approaches 90° compared to grades closer to 180°. Therefore, chaotic flow occurs at the neck section, increasing interfacial area and facilitating mixing. It suggests that the difference in neck angles influences M_n.

To investigate the correlation between M_n and the width ratio of the microchannel, we conducted mixing experiments and compared the M_n in toroidal micromixers with varying width ratios. In the toroidal micromixer with width ratios of 3.0 and 4.0, M_n values achieving 0.99 were observed at approximately 2.0 ms. However, mixing was not complete in the toroidal micromixers with width ratios of 1.0 and 2.0, with M_n values of 0.89 and 0.96, respectively. For both designs, even at the endpoint, the M_n values were not reached 1.0 (Fig. 4c). In particular, with a width ratio of 4.0, the mixing of the two fluids was confirmed at 1.4 ms, while the ratio of 1.0 did not mix, and the boundary between the two fluids was visible (Fig. 4d). This indicates that, as the width ratio increases, the M_n reaches 1.0 within a short time. In the toroidal micromixer, when the width ratio is varied, one fluid enters the wider side of the channel with the other fluid, increasing the contact area between the fluids. This leads to enhanced mixing as the interface area increases, and there is an increase in imbalanced collisions at the recombination neck section, resulting in improved M_n. In contrast, when the width ratio of the channel is the same, the two fluids symmetrically enter the channel, leading to reduced imbalanced collisions and limiting the M_n [45, 49].

As a result, we confirmed that in the design of the toroidal micromixer, lower neck angles and larger width ratios lead to improved M_n. Among the toroidal designs, we identified the micromixer with a neck angle of 90° and a width ratio 4.0 as the most efficient design.

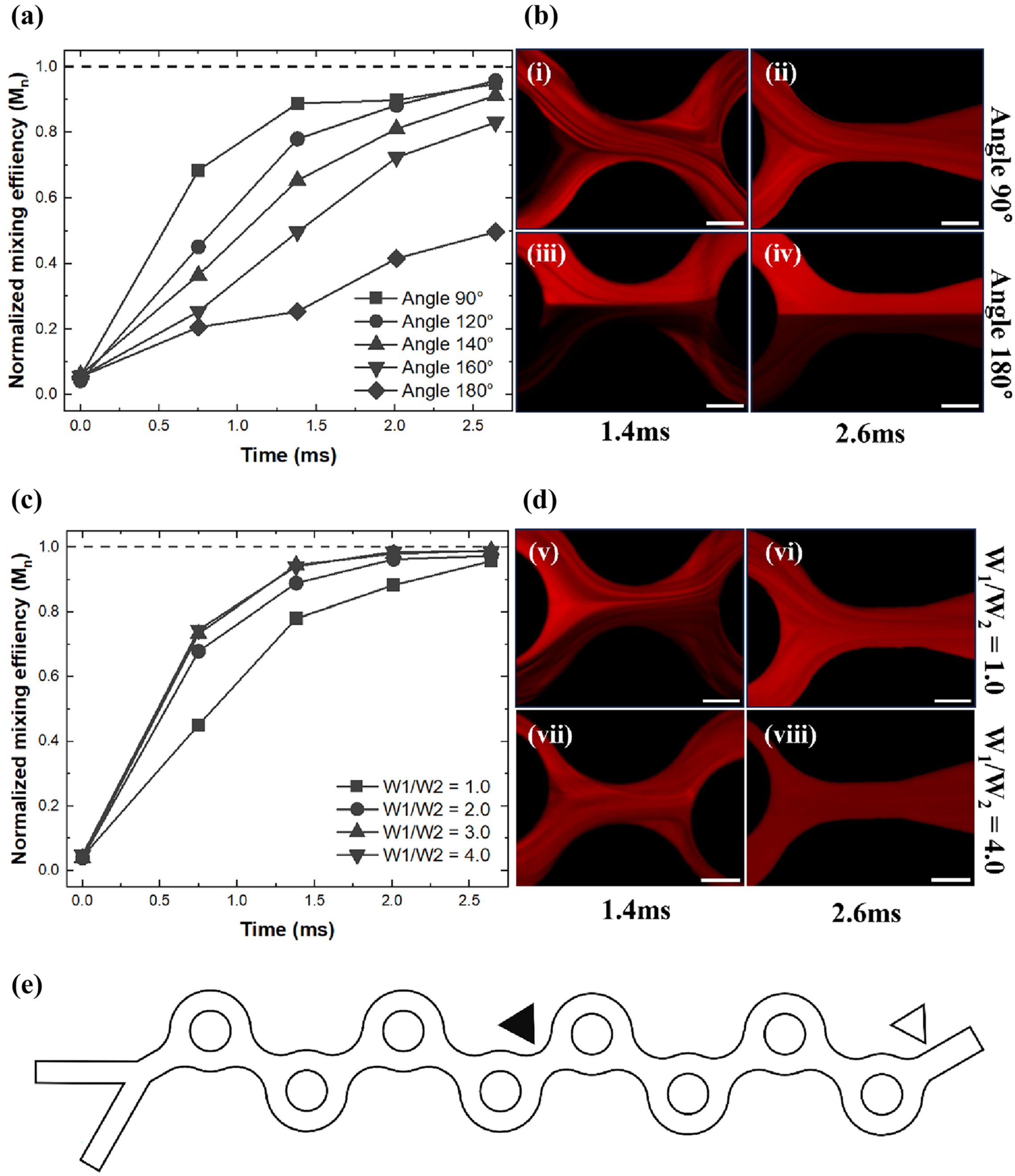

Fig. 4 Investigation of various designs to evaluate the influence of neck angle and width ratio on a toroidal micromixer. **a** Comparison of normalized mixing efficiency in toroidal micromixer with different neck angle. **b** Fluorescence images illustrating variations in mixing across different toroidal mixers with different two neck angles. (i) and (iii) are the fluorescence images at 1.4 ms. (ii) and (iv) are the fluorescence images at 2.6 ms. **c** Comparison of normalized mixing efficiency in toroidal micromixer with different width ratio. **d** Fluorescence images showing variations in mixing across different toroidal mixers with different width ratios. (v) and (vii) are the fluorescence images at 1.4 ms. (vi) and (viii) are the fluorescence images at 2.6 ms. **e** Schematic diagram of the measurement points in toroidal micromixer. The closed triangles represent 1.4 ms, while the open triangles indicate 2.6 ms (scale bar size = 100 µm)

Comparison of Mixing Efficiency in 3D Zig-Zag Micromixer with and Without Junction

In Fig. 2, we confirmed that the 3D zig-zag micromixer is the most efficient. However, we observed a significantly lower M_n at 0.4 ms than other micromixers. We anticipated this due to the absence of junctions when entering the mixing region from the inlet in the 3D zig-zag structure. Therefore, we compared the 3D zig-zag micromixer with and without a junction at the inlet (Fig. 5a).

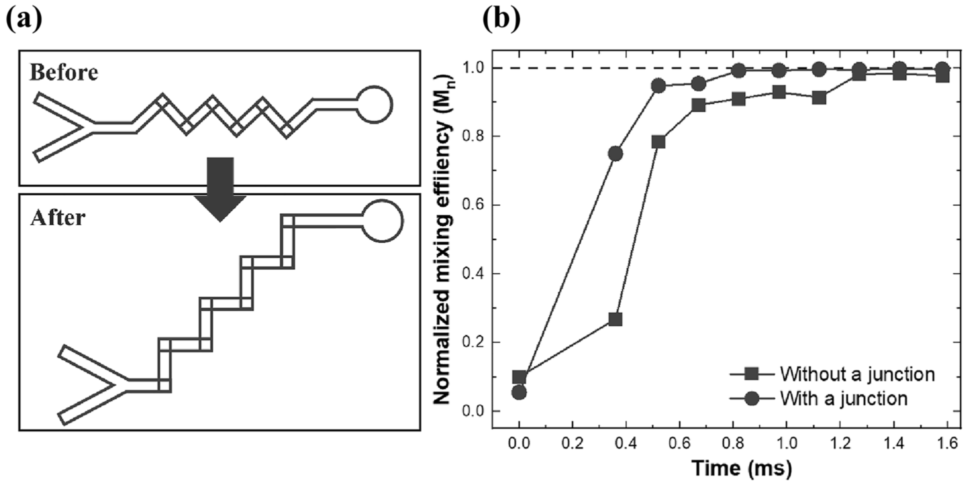

Fig. 5 Difference in mixing efficiency before and after modification of the design in the 3D zig-zag micromixer. **a** Scheme of 3D zig-zag micromixer with and without a junction. **b** Comparison of normalized mixing efficiency in a 3D zig-zag micromixer

To evaluate the M_n, we obtained fluorescence images by designating the middle of each channel in the 3D mixer as an ROI. Then, we calculated the average fluorescence intensity and standard deviation from the fluorescence images.

In both designs, with and without a junction at the inlet, the M_n value increases sharply at the initial junction. However, the design with a junction was observed to mix more rapidly (Fig. 5b).

When compared the M_n value at 0.4 ms between the designs with and without a junction, the design without a junction exhibited approximately 0.27, while the design with a junction improved to approximately 0.75. This indicates that the design with a junction at the inlet achieved enhanced M_n value at the same time.

In addition, the design without a junction required approximately 1.3 ms to reach the M_n value of 1.0, while the design with a junction reached it at approximately 0.8 ms. The mixing time can be reached about 0.5 ms faster than the design without a junction, resulting in an improvement of approximately 38%. This demonstrates that the additional junction induced secondary flow, allowing for more efficient mixing. In conclusion, in the design of the 3D zig-zag micromixer, the configuration with an additional junction at the inlet proved to be the most efficient design.

Comparative Analysis of Mixing Efficiency in Toroidal and 3D Zig-Zag Micromixers

Ultimately, we compared the M_n of the toroidal micromixer and 3D zig-zag micromixer to identify the most efficient micromixer design (Fig. 6). The comparison of M_n between the two micromixers revealed that the 3D zig-zag micromixer is a more efficient design. The toroidal micromixer achieved a M_n value of 1.0 within about 2 ms. However, using the 3D zig-zag micromixer achieving an M_n value 1.0 in a short time of 0.8 ms. This indicates that the 3D zig-zag micromixer exhibited a significant improvement of about 60% compared to the toroidal micromixer, demonstrating superior mixing performance.

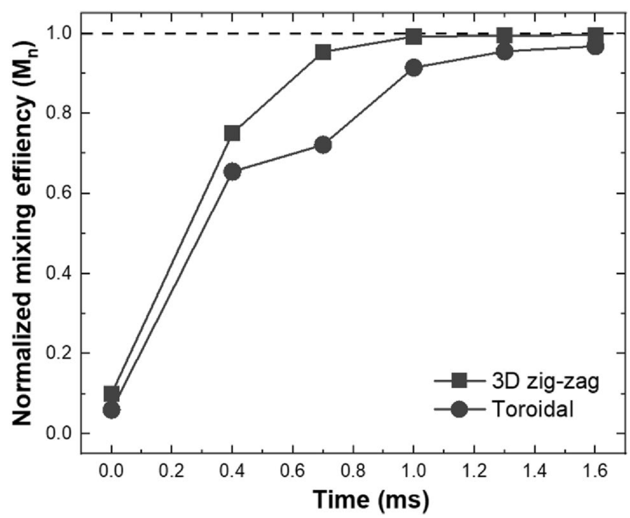

Fig. 6 Graph of normalized mixing efficiency between the final design of 3D zig-zag and toroidal micromixers

The difference in M_n is attributed to the toroidal micromixer having two-dimensional structure, while the 3D zig-zag micromixer has three-dimensional structure. In the case of the toroidal structure, mixing is confined to the x–y plane, whereas in the 3D zig-zag structure, in addition to the primary flow in the *x*–*y* plane, secondary flow occurs along the *z*-axis. This multi-dimensional fluid motion contributes to increased interfacial area, resulting in enhanced M_n compared to the toroidal micromixer.

Based on these results, we compare the M_n value of the 3D zig-zag micromixer with that of other micromixers. Table 3 presents a comparison of the M_n among five different micromixers. The toroidal micromixer features a design with a neck angle of 90° and a width ratio of 1.0, while the

Table 3 Normalized mixing efficiency values at 1.0 ms for various micromixers

Micromixer design	Straight	Herring-bone	Serpentine	Toroidal	3D zig-zag
Normalized mixing index	0.02	0.48	0.72	0.91	0.99

3D zig-zag micromixer incorporates a design with junctions. When compared at a mixing tine of 1.0 ms, other micromixers, excluding the 3D zig-zag micromixer, did not reach the fully mixed value of 1.0. These results indicate that the comparison of M_n among different micromixers revealed that the mixing in the 3D zig-zag micromixer is the most efficient. And this attains an M_n value of 1.0 within a short time of 0.8 ms.

Estimation of Mixing in 3D Zig-Zag Micromixer with Different Reynolds Number

We investigated the M_n in the 3D zig-zag micromixer at different Reynolds numbers. Furthermore, we visualized the fluid flow along each junction using a confocal laser scanning microscope to observe the extent of fluid mixing.

Figure 7a shows the comparing normalized M_n in the 3D zig-zag micromixer at different Reynolds numbers. All variables except for the flow rate were fixed, and as a result, the Reynolds number increased with the flow velocity within the micromixer.

The results showed that as the Reynolds number decreased, the M_n also reduced. Conversely, an increase in the Reynolds number correlates with an upward trend in M_n. This indicates that at low Reynolds numbers, the mixing of fluids in the micromixer occurs slowly, decreasing in M_n. In contrast, as the Reynolds number increases, turbulence is induced in the fluid, resulting in an upward trend in M_n. As shown in the figure, except the case of Re = 17, we observed that the M_n value reached 1.0 at all other Reynolds numbers. Particularly, at Re = 332 and Re = 449, the M_n value reached 1.0 at 2.7 mm. These results imply the impact of flow velocity on Reynolds number.

Additionally, we visualized the mixing at the middle of each channel in a 3D zig-zag micromixer, and the fluid velocity fixed at Re = 332 (Fig. 7b). In the first cross-section (1.2 ms), we observed that the fluids remained unmixed. However, starting from the second cross-section (2.2 ms), mixing occurred, resulting in a uniform mixture.

In conclusion, in the 3D zig-zag micromixer, there was a trend of rapid increase of M_n at higher Reynolds numbers. When examining the cross-sectional area, it was confirmed that the two fluids are uniformly mixed.

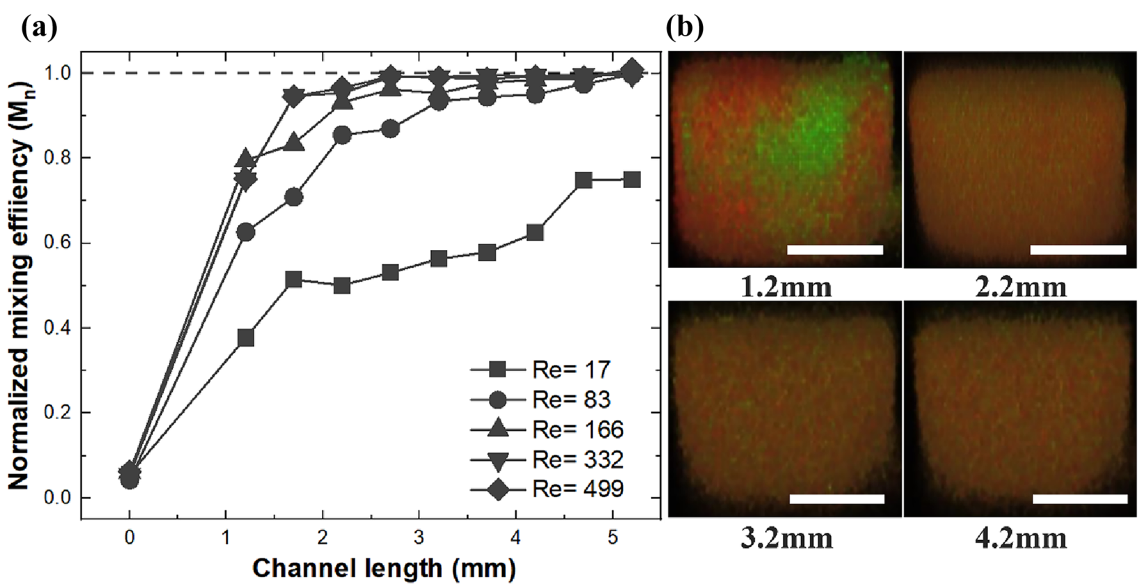

Fig. 7 Effect of Reynolds numbers on mixing efficiency. **a** Comparison of normalized mixing efficiency in 3D zig-zag micromixer at different Reynolds numbers. **b** 3D confocal fluorescence images for visualizing cross-sections of a 3D zig-zag micromixer (***Re*** = 332). Scale bar size = 100 µm

Conclusions

Efficiently achieving high mixing efficiency within a short time in microfluidic devices is a critical technology in chemistry and biological reactions. To address this challenge, numerous researchers have proposed various designs for micromixers. In this paper, we compare various passive micromixer designs and propose a micromixer design that effectively achieves rapid mixing quickly. To confirm the most efficient design in a passive micromixer, designs for straight, serpentine, herringbone, toroidal and 3D zig-zag micromixers were developed and compared for M_n. As a result, it was confirmed that toroidal and 3D zig-zag micromixer achieved more efficient mixing compared to other micromixers. Additionally, we identified the parameters influencing the M_n of the toroidal and 3D zig-zag micromixer. The most effective designs for each micromixer were determined, and the M_n was compared among the final designs of each micromixer.

Ultimately, the 3D zig-zag micromixer was identified for exhibiting the highest M_n, with secondary mixing flows occurring along the z-axis. This result demonstrates the capability of achieving effective mixing in a short time, approximately 0.8 ms. Through this study, the proposed 3D zig-zag micromixer is expected to find valuable applications, particularly in efficiently conducting chemical reactions with small amounts of reagents or promoting reactions by mixing reagents in medical diagnostics and testing. Especially for the mRNA-LNP vaccines, aimed at relieving the world from a tragic global pandemic, where the uniform formation of nanoparticles and nanostructures is crucial, a rapid mixing process is essential. The 3D zig-zag micromixer introduced in this paper is expected to be highly beneficial, as it can achieve a high M_n quickly, making it suitable for various applications.

Acknowledgements This research was supported by the National Research Foundation of Korea (NRF) grant funded by the Korea government (MSIT) (No. 2021R1A2C3004936 and 2021R1A5A8032895). ※ MSIT: Ministry of Science and ICT.

References

1. J.-C. Leong, C.-H. Tsai, C.-L. Chang, C.-F. Lin, L.-M. Fu, Rapid microfluidic mixers utilizing dispersion effect and interactively time-pulsed injection. Jpn. J. Appl. Phys. **46**, 5345 (2007)
2. T.H. Schulte, R.L. Bardell, B.H. Weigl, Microfluidic technologies in clinical diagnostics. Clin. Chim. Acta **321**, 1–10 (2002)
3. S.Z. Razzacki, P.K. Thwar, M. Yang, V.M. Ugaz, M.A. Burns, Integrated microsystems for controlled drug delivery. Adv. Drug Deliv. Rev. **56**, 185–198 (2004)
4. Y. He et al., Numerical investigation of the mixing process in a Twin Cam Mixer: influence of triangular cam height-base ratio and eccentricity. Korean J. Chem. Eng. **38**, 552–564 (2021)
5. A.G. Niculescu, C. Chircov, A.C. Birca, A.M. Grumezescu, Fabrication and applications of microfluidic devices: a review. Int. J. Mol. Sci. **22**(4), 2011 (2021).
6. I. Ji, J.W. Kang, T. Kim, M.S. Kang, S.B. Kwon, J. Hong, 3D printing-based ultrafast mixing and injecting systems for time-resolved serial femtosecond crystallography. Korean Chem. Eng. Res. **60**(2), 300–307 (2022)
7. S.-H. Jang, I.-J. Kang, Drug delivery study on chitosan nanoparticles using iron oxide (II, III) and valine. Korean Chem. Eng. Res. **59**, 514–520 (2021)
8. W.-H. Choi, B. Kim, Fabrication and characterization of dissolving microneedles containing lecithin for transdermal drug delivery. Korean Chem. Eng. Res. **59**, 429–434 (2021)
9. M. Maeki, S. Uno, A. Niwa, Y. Okada, M. Tokeshi, Microfluidic technologies and devices for lipid nanoparticle-based RNA delivery. J. Control. Release **344**, 80–96 (2022)
10. K.K.V. Canlas et al., Trends in nano-platforms for the treatment of viral infectious diseases. Korean J. Chem. Eng. **40**, 706–713 (2023)
11. E. Hong, J. Jeon, H.U. Kim, Recent development of machine learning models for the prediction of drug-drug interactions. Korean J. Chem. Eng. **40**, 276–285 (2023)
12. G. Zhang, J. Sun, Lipid in chips: a brief review of liposomes formation by microfluidics. Int. J. Nanomed. **16**, 7391–7416 (2021).
13. M. Maeki, N. Kimura, Y. Sato, H. Harashima, M. Tokeshi, Advances in microfluidics for lipid nanoparticles and extracellular vesicles and applications in drug delivery systems. Adv. Drug Deliv. Rev. **128**, 84–100 (2018)
14. M.S. Ali, N. Hooshmand, M. El-Sayed, H.I. Labouta, Microfluidics for development of lipid nanoparticles: paving the way for nucleic acids to the clinic. ACS Appl. Bio Mater. **6**, 3566–3576 (2021)
15. M. Faryadi, M. Rahimi, S. Safari, N. Moradi, Effect of high frequency ultrasound on micromixing efficiency in microchannels. Chem. Eng. Process. **77**, 13–21 (2014)
16. K.-I. Min, Fabrication of 3D multilayered microfluidic channel using fluorinated ethylene propylene nanoparticle dispersion. Korean Chem. Eng. Res. **59**, 639–643 (2021)
17. B. Zhou et al., Design and fabrication of magnetically functionalized flexible micropillar arrays for rapid and controllable microfluidic mixing. Lab Chip **15**, 2125–2132 (2015)
18. D. Ahmed, X. Mao, J. Shi, B.K. Juluri, T.J. Huang, A millisecond micromixer via single-bubble-based acoustic streaming. Lab Chip **9**, 2738–2741 (2009)
19. K. Karthikeyan, L. Sujatha, Study of permissible flow rate and mixing efficiency of the micromixer devices. Int. J. Chem. React. Eng. **17**, 20180047 (2018)
20. A. Cosentino et al., An efficient planar accordion-shaped micromixer: from biochemical mixing to biological application. Sci. Rep. **5**, 17876 (2015)
21. A. Agarwal, A. Salahuddin, H. Wang, M.J. Ahamed, Design and development of an efficient fluid mixing for 3D printed lab-on-a-chip. Microsyst. Technol. **26**, 2465–2477 (2020)
22. H. Lv, X. Chen, Novel study on the mixing mechanism of active micromixers based on surface acoustic waves. Ind. Eng. Chem. Res. **61**, 10264–10274 (2022)
23. M. Bayareh, M.N. Ashani, A. Usefian, Active and passive micromixers: a comprehensive review. Chem. Eng. Process. Process Intens. **147**, 107771 (2020)
24. J. Sun et al., Numerical and experimental investigation of a magnetic micromixer under microwires and uniform magnetic field. J. Magn. Magn. Mater. **551**, 169141 (2022)
25. D. Bahrami, A.A. Nadooshan, M. Bayareh, Effect of non-uniform magnetic field on mixing index of a sinusoidal micromixer. Korean J. Chem. Eng. **39**, 316–327 (2022)

26. S.-G. Jeong et al., Nanoliter scale microloop reactor with rapid mixing ability for biochemical reaction. Korean J. Chem. Eng. **35**, 2036–2042 (2018)
27. B. Yin et al., Micromixer with fine-tuned mathematical spiral structures. ACS Omega **6**, 30779–30789 (2021)
28. E. Nady, G. Nagy, R. Huszánk, Improvement in mixing efficiency of microfluidic passive mixers functionalized by microstructures created with proton beam lithography. Chem. Eng. Sci. **247**, 117006 (2022)
29. S. Hossain, M. Ansari, K.-Y. Kim, Evaluation of the mixing performance of three passive micromixers. Chem. Eng. J. **150**, 492–501 (2009)
30. J. Choe, Y. Kwon, Y. Kim, H.-S. Song, K.H. Song, Micromixer as a continuous flow reactor for the synthesis of a pharmaceutical intermediate. Korean J. Chem. Eng. **20**, 268–272 (2003)
31. M. Nimafar, V. Viktorov, M. Martinelli, Experimental comparative mixing performance of passive micromixers with H-shaped sub-channels. Chem. Eng. Sci. **76**, 37–44 (2012)
32. V. Viktorov, M.R. Mahmud, C. Visconte, Comparative analysis of passive micromixers at a wide range of Reynolds numbers. Micromachines **6**, 1166–1179 (2015)
33. P. Li, J. Cogswell, M. Faghri, Design and test of a passive planar labyrinth micromixer for rapid fluid mixing. Sens. Actuat. B Chem. **174**, 126–132 (2012)
34. T. Tofteberg, M. Skolimowski, E. Andreassen, O. Geschke, A novel passive micromixer: lamination in a planar channel system. Microfluid. Nanofluid. **8**, 209–215 (2010)
35. J.J. Chen, Y.S. Shie, Interfacial configurations and mixing performances of fluids in staggered curved-channel micromixers. Microsyst. Technol. **18**, 1823–1833 (2012)
36. M.K. Parsa, F. Hormozi, D. Jafari, Mixing enhancement in a passive micromixer with convergent–divergent sinusoidal microchannels and different ratio of amplitude to wave length. Comput. Fluids **105**, 82–90 (2014)
37. X. Chen, Z. Zhao, Numerical investigation on layout optimization of obstacles in a three-dimensional passive micromixer. Anal. Chim. Acta **964**, 142–149 (2017)
38. S.O. Hong et al., Gear-shaped micromixer for synthesis of silica particles utilizing inertio-elastic flow instability. Lab Chip **21**, 513–520 (2021)
39. S. Kim et al., Monolithic 3D micromixer with an impeller for glass microfluidic systems. Lab Chip **20**, 4474–4485 (2020)
40. A.D. Stroock et al., Chaotic mixer for microchannels. Science **295**, 647–651 (2002)
41. Wild, Andre, Timothy Leaver, and Robert James Taylor. "Bifurcating mixers and methods of their use and manufacture." U.S. Patent No. 10,076,730. (2018)
42. H. Kim et al., Submillisecond organic synthesis: Outpacing Fries rearrangement through microfluidic rapid mixing. Science **352**, 691–694 (2016)
43. B. Lee et al., Characterization of passive microfluidic mixer with a three-dimensional zig-zag channel for cryo-EM sampling. Chem. Eng. Sci. **281**, 119161 (2023)
44. C. Wang, Y. Hu, Mixing of liquids using obstacles in y-type microchannels. J. Appl. Sci. Eng. **13**, 385–394 (2010)
45. M.A. Ansari, K.-Y. Kim, Shape optimization of a micromixer with staggered herringbone groove. Chem. Eng. Sci. **62**, 6687–6695 (2007)
46. T.J. Kwak et al., Convex grooves in staggered herringbone mixer improve mixing efficiency of laminar flow in microchannel. PLoS ONE **11**, e0166068 (2016)
47. P.B. Howell Jr., D.R. Mott, J.P. Golden, F.S. Ligler, Design and evaluation of a Dean vortex-based micromixer. Lab Chip **4**, 663–669 (2004)
48. C. Webb et al., Using microfluidics for scalable manufacturing of nanomedicines from bench to GMP: a case study using protein-loaded liposomes. Int. J. Pharm. **582**, 119266 (2020)
49. J. Li, G. Xia, Y. Li, Numerical and experimental analyses of planar asymmetric split-and-recombine micromixer with dislocation sub-channels. J. Chem. Technol. Biotechnol. **88**, 1757–1765 (2013)